Quantitative Three-Dimensional Analysis of Embryonic Chick Morphogenesis Via Microcomputed Tomography

JUN SUP KIM, JOUHA MIN, ANDREW K. RECKNAGEL, MARK RICCIO, AND JONATHAN T. BUTCHER*

Department of Biomedical Engineering, Cornell University, Ithaca, New York

ABSTRACT

Embryonic development is a remarkably complex and rapidly evolving morphogenetic process. Although many of the early patterning events have been well described, understanding the anatomical changes at later stages where clinically relevant malformations are more likely to be survivable has been limited by the lack of quantitative 3D imaging tools. Microcomputed tomography (Micro-CT) has emerged as a powerful tool for embryonic imaging, but a quantitative analysis of organ and tissue growth has not been conducted. In this study, we present a simple method for acquiring highly detailed, quantitative 3D datasets of embryonic chicks with Micro-CT. Embryos between 4 and 12 days (HH23 and HH40) were labeled with osmium tetroxide (OT), which revealed highly detailed soft tissue anatomy when scanned at 25 μm resolution. We demonstrate tissue boundary and inter-tissue contrast fidelity in virtual 2D sections are quantitatively and qualitatively similar to those of histological sections. We then establish mathematical relationships for the volumetric growth of heart, limb, eye, and brain during this period of development. We show that some organs exhibit constant exponential growth (eye and heart), whereas others contained multiple phases of growth (forebrain and limb). Furthermore, we show that cardiac myocardial volumetric growth differs in a time and chamber specific manner. These results demonstrate Micro-CT is a powerful technique for quantitative imaging of embryonic growth. The data presented here establish baselines from which to compare the effects of genetic or experimental perturbations. Quantifying subtle differences in morphogenesis is increasingly important as research focuses on localized and conditional effects. Anat Rec, 294:1–10, 2011. © 2010 Wiley-Liss, Inc.

Key words: quantitative imaging; morphology; embryo; chick; histology quantification; microCT-based virtual histology

Congenital malformations remain a significant cause of death and disability. Although many birth defects have an underlying genetic mutation, the majority of clinical cases are not traceable to a genetic cause (McBride et al., 2005; Clark et al., 2006). Molecular biology based research over the last decade has uncovered numerous transcription factors, signaling networks, and matricellular proteins essential in controlling embryonic morphogenesis (Camenisch et al., 2002; Niswander, 2002; Borue and Noden, 2004; Olson, 2004), but deficiencies in

Grant sponsor: American Heart Association (Scientist Development); Grant number: 0380384N; Grant sponsor: NYSTAR Center for Advanced Technology.

*Correspondence to: Jonathan T. Butcher, Department of Biomedical Engineering, 304 Weill Hall, Cornell University, Ithaca, NY 14853. Tel: 607-255-3575. Fax: 607-255-7330.
E-mail: jtb47@cornell.edu

Received 18 June 2010; Accepted 25 August 2010

DOI 10.1002/ar.21276
Published online 2 December 2010 in Wiley Online Library (wileyonlinelibrary.com).

many of these proteins lead to early embryonic lethality (particularly in the heart) that would not be recognized or treatable clinically. Embryonic development also progresses at the cellular, tissue, and organ levels, all of which are highly sensitive to changes in environmental signaling such as through mechanical or tissue perturbation (Hogers et al., 1999; Munoz-Sanjuan et al., 1999; Maciaczyk et al., 2009). Understanding the relationships between forming structures and their microenvironment are critically important to developing strategies to combat and counteract these serious clinical problems. Analysis of and experimentation with small animal model systems such as the chick and mouse have been crucial components for expanding knowledge of developmental biology. Quantitative imaging is an increasing need in basic science research as morphological consequences of conditional mutations and microscale environmental alterations initiate subtle but progressive malformations that resemble clinically relevant defects. Furthermore, evidence suggests that relatively minor malformations that may not have received attention may have significant consequences later in life (Snider et al., 2008). Identifying and characterizing these during embryonic development can lead to better predictors of future performance. Traditionally, identifying defects has been a tedious process relying on thin section histology. Analysis of 3D events with 2D images (as in this technique) is problematic because of (A) nonlinear tissue shrinkage effects with embedding and (B) significant limitations in out-of-plane resolution that are further compounded by even small differences in sectioning angle. 3D reconstruction of serial sections is the most straightforward way to overcome these limitations, but complex and tortuous geometries common in embryonic development are often poorly resolved unless nearly every section is retained, dramatically increasing time required (Williams and Doyle, 1996).

Intrinsically 3D digital imaging technologies have been promoted to fill this need. The most developed and utilized of which is microscopic magnetic resonance imaging (μMRI). Early attempts with low field strength coils gave poor resolution (Smith et al., 1996; Dhenain et al., 2001). More recently, 9.4T and greater strength coils have generated 3D resolution images under 30 μ is possible (Zhang et al., 2003; Ruffins et al., 2007). High field strength μMRI machines, however, are of limited availability because of their extreme expense (>$3 Million) and require upwards of 30 hr of scan time, which is largely cost prohibitive for routine phenotype screening (Dhenain et al., 2001). Image atlases of whole embryo development have been created for chick (Bain et al., 2007; Li et al., 2007), quail (Ruffins et al., 2007; Hogers et al., 2009), and mouse (Dhenain et al., 2001; Johnson et al., 2006), but resolution and contrast strength remains challenging for earlier embryos. In the case of the chick, the earliest stage whole embryo 3D image data to date is Day 8, long after many morphogenic processes have occurred (Li et al., 2007).

Micro-Computed Tomography (Micro-CT), which images structures by X-Ray attenuation, is an attractive technology because of its much lower capital cost in comparison to MRI (<$500,000), fast acquisition times, and high spatial resolution within a significantly larger scan field. We and others used an injectable CT dense casting agents to visualize cardiovascular lumen development in chick embryos (Butcher et al., 2007b; Hu et al., 2009; Wang et al., 2009). More recently, we demonstrated using osmium tetroxide (OT) as a diffusive CT contrast agent that high resolution detailed visualization and segmentation of rodent embryos to newborns was possible with Micro-CT; these previous studies included early stage mouse and rabbit embryos (Johnson et al., 2006; Carney et al., 2007; Martinez et al., 2009). Investigators have since followed with related studies in model organisms to explore the effects of different chemical agents on soft tissue contrast enhancement (Metscher, 2009; Degenhardt et al., 2010).

Despite the recent progress made with Micro-CT imaging of embryos, quantitative analyses of 3D datasets generated by this technique have not been performed. Previous studies have investigated volumetric organ growth in rodent embryos (Goedbloed, 1972, 1980), but very limited information exists for chick. In this study, we present protocols for Micro-CT imaging across a large range of morphogenic activity in the embryonic chick. We show that Micro-CT produces 3D datasets with virtual 2D slices with similar image quality as histological sections for chick embryos as early as Day 4 (HH21). Using this digital database we establish growth curves for whole chick embryos and key organs (heart, eye, limbs, and brain). The combination of enhanced soft tissue structural detail and ease of quantitative analysis make Micro-CT a useful system for rapid screening of morphological changes, a continued need for developmental biology research.

MATERIALS AND METHODS

Embryo Preparation

Fertilized white leghorn eggs were incubated at 38°C, 55% humidity for times ranging from 4 to 12 days (HH23 to HH40). Four to ten specimens were processed for each developmental stage. Eggs were cracked into polystyrene culture dishes, and the embryos were retrieved and fixed in 10% buffered formalin overnight at room temperature. Embryos were incubated overnight in a solution of 0.1 M sodium cacodylate (pH 7.2), 1% glutaraldehyde, and 1% osmium tetroxide (OT) rocking at room temperature as previously described (Johnson et al., 2006). OT is extremely volatile and toxic, so all procedures were performed with extreme care in ventilated fume hoods, using secondary containers whenever possible. After washing in 0.1 M sodium cacodylate buffer, embryos were incubated in OT solution for an additional 6 hr at 4°C to allow diffusion into the tissue. Vitelline vein or intracardiac perfusion of OT was additionally performed in embryos later than Day 8 to ensure homogeneous distribution without tissue distension (Zhang et al., 2003). The reaction was quenched by rinsing twice in 0.1 M cacodylate Buffer for 30 min. Specimens were dehydrated in 25%, 50%, 75%, and 100% graded ethanol in phosphate-buffered saline for 30 min each. Afterwards, specimens were packed in standard 15 or 50 mL polypropylene tubes separated with loose sponges and filled with ethanol.

Imaging

Specimen tubes were transferred to the micro-CT imaging system (GE eXplore CT120, GE Healthcare)

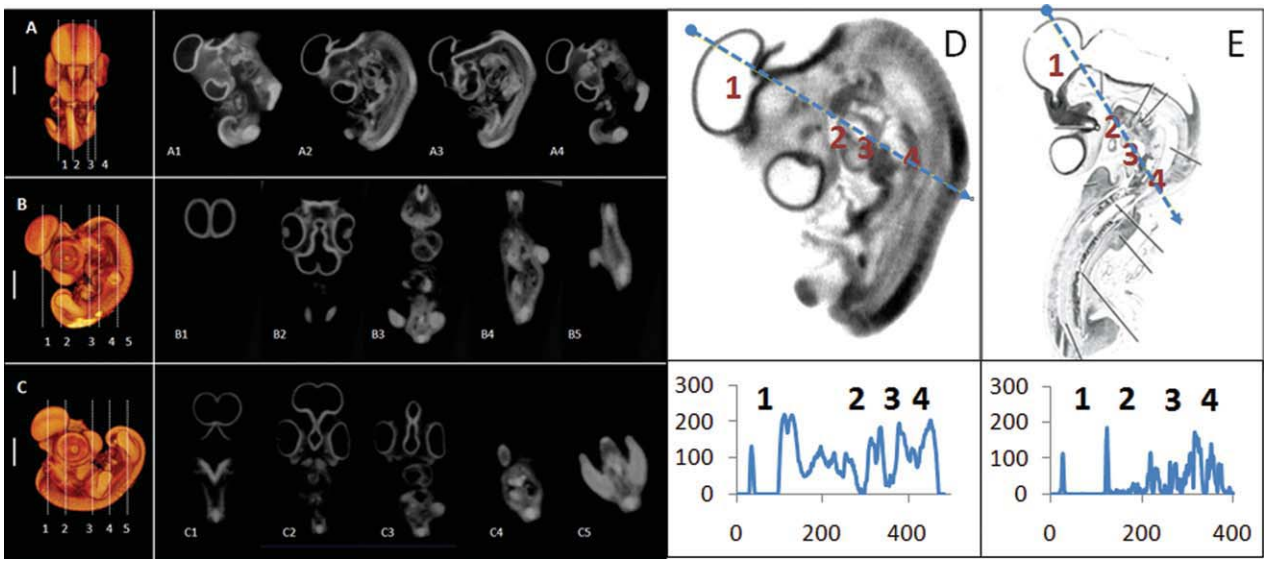

Fig. 1. 3D surface rendering and 2D digital sections of Day 4 chick embryos. Left panels are 3D isosurface renderings. Middle panels are 2D sections in (**A1**–**A4**) Sagittal, (**B1**–**B5**) coronal, and (**C1**–**C5**) axial planes. Right panels compare signal contrast of Micro-CT (**D**) with histology (**E**). Graphs below images contrast along lines in D and E, respectively. 1 = forebrain, 2 = outflow tract, 3 = ventricle, 4 = somites. Scale bars (A, B, and C) = 1 mm.

and held in place with foam guides. The field of view of this instrument is 45 × 45 × 45 mm, well suitable for embryonic chicks. Volumetric imaging of embryos was performed by rotating the 10 Megapixel camera 360° (1°/step), averaging two images per step, resulting in 25 μm isometric spatial resolution. Image stacks were then processed and reconstructed into 3D datasets using GE internal reconstruction software. The entire process took ~2 hr for each specimen tube (which contained up to five embryos). Post-processing, visualization, and image quantification was then performed using Microview (GE healthcare) and Osirix (Osirix). From these, 3D isosurface renderings and virtual 2D slices were generated.

Segmentation and Quantification

3D Image volume segmentations were performed using a region growing algorithm (RGA, Osirix). User-defined seed points are positioned in a region of interest (often a single segment/organ), and a statistical analysis is made of the gradient magnitude in the local neighborhood to find the standard deviation (Wenink, 1992). The resulting structures were saved as separate volumes, which could also be recombined into a single volume. In some cases, artificial boundaries were scribed so that the RGA propagated only within the anatomical region of interest (e.g., so that the segmentation did not extend out of the ventricle into the atrium). For most of the quantitative calculations present in this article, the organ or region of interest was segmented by creating negative space (i.e., setting pixel values in that region to zero contrast) and propagating that negative space through the Z plane. In this way, we captured only one tissue type (i.e., heart, brain, wing bud) and could independently quantify tissue or fluid volume in a particular organ. Multiple labeled volumes were derived from each embryo and quantified in the same way. Data from at least three embryos were used for each region/tissue. Statistical analysis was performed using ANOVA followed by post hoc testing using $P < 0.05$ as a significance threshold.

RESULTS

Comparison of Micro-CT with Histology

Surface and internal morphology were imaged and quantified at three stages of development (Days 4, 7, and 10). These were chosen because they encompass limb bud extension to digit formation, neural tube differentiation into specific brain cavities, and the development of the four chambered heart from an initially linear tube all occur during this window. Three-dimensional volumes were created from each dataset, and virtual frontal, sagittal, and transverse sections were made at different depths through the embryo. Micro-CT sensitivity in visualizing tissue boundaries, tissue specific contrast, and anatomical landmarks were quantified in comparison to histological sections obtained from a published atlas (Bellairs and Osmond, 2005). Virtual sections from Day 4 embryos (HH23, Fig. 1) verified complete penetration after 6 hr. Many internal tissue structures could be differentiated from each other via contrast, particularly at interfacial boundaries. Typical staging anatomical landmarks were easily distinguished, including the head, eye, limbs, and tail. Internal structural morphology that is often affected by genetic or environmental insults was also visible, such as somites, liver, non-septated heart tube and cardiac cushions (atrioventricular not outflow), dorsal aorta, neural tube, and pharyngeal arches. Structures that were too small to be visualized by Micro-CT at this stage included the internal microvessels of the embryo (smaller than the major arteries and veins entering and leaving the heart), and the primitive gastro-intestinal tract. Section histology was somewhat sharper than Micro-CT for boundary

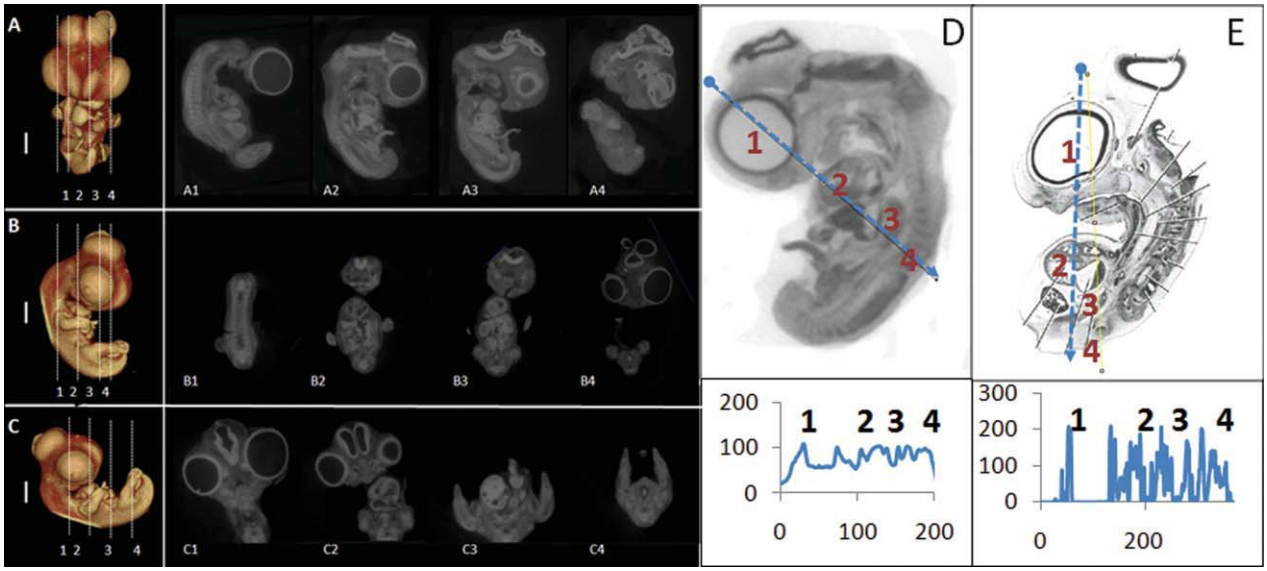

Fig. 2. 3D surface rendering and 2D digital sections of Day 7 chick embryos. Left panels are 3D isosurface renderings. Middle panels are 2D sections in (**A1**–**A4**) Sagittal, (**B1**–**B4**) coronal, and (**C1**–**C4**) axial planes. Right panels compare signal contrast of Micro-CT (**D**) with histology (**E**). Graphs below images contrast along lines in D and E, respectively. 1 = eye, 2 = ventricle, 3 = limb, 4 = sclerotome. Scale bars (A, B, and C) = 1 mm.

detection, but Micro-CT gave better signal intensity for non-boundary regions. Section histology of course gives greater cellular resolution limited only by the optics applied.

Significantly more anatomical complexity is developed by Day 7 (HH30, Fig. 2), much of which is visualized by Micro-CT. Traditional exterior anatomical landmarks like eyes, bent wings, mandible, and beak are clearly distinguished. Separate atria and ventricles were clearly delineated, with valves (inflow and outflow) and septal structures now visible. Internal structures were identifiable in virtual sections both by tissue boundaries that exhibited enhanced local contrast and by relative core tissue contrast. These include liver, umbilical artery, esophagus, trachea, lung buds, sclerotomes and spinal cord, gizzard, and numerous arterial networks (vessels larger than 100 μm in diameter). Comparison to similarly staged section histology shows that while histological sections gave better discrimination of tissue boundaries and intra-tissue contrast, Micro-CT imaging is qualitatively similar. There was an increase in basal contrast in the OT treated embryo at this stage, which suggests that as embryonic tissue condenses differential diffusion occurs to a lesser degree.

At Day 8 (HH32) and later (Fig. 3), OT diffusion through the epidermis was severely impaired. For these stages, the embryo was then first perfused with OT through the apex of the heart before also applying the passive diffusion protocol. As before, anatomical landmarks such as the eyes, digited limbs, neck, tail, and feather buds were all visible. As seen in virtual sections, internal structures such as the metanephros, mesonephros, lung branches, lens, heart, telencephalon, and choroid plexus. More complex meso-scale structural features within many organs were rendered in virtual sections, which reflected organotypic maturation. The complete cardiac outflow tract anatomy (including pharyngeal/aortic arches) was now clearly visible and could be continuously rendered three dimensionally. Some pockets of tissue remained poorly perfused, primarily in the head and abdomen. These may reflect regions that are still poorly vascularized at this stage. Generally, Micro-CT generated sections were comparable to section histology at 25 μ or larger scales. The increased basal tissue contrast seen in Day 7 preparations was also present here, but interfacial boundaries were still easily distinguishable and in the same positions when compared to histological sections.

Quantitative Volumetric Analysis of Chick Embryonic Development

Three-dimensional quantitative segmentation was performed on specific organs: brain, wing, leg, eye, and heart from Day 4 through Day 10 (Fig. 4A–C). The region grow algorithm was applied to quantify stage specific tissue volumes pixel by pixel, while rendering each organ with a different color. The process took <5 min to perform. Generally, we found nonlinear growth patterns in the developing embryo that in some cases exhibited stage specific transitions. We determined regressions for each organ as suggested by Goedbloed (Goedbloed, 1980), which are shown in Table 1. Whole Embryo growth was exponential over the full range of development assayed (Days 4–10) without any significant changes in rate (Fig. 4D). Total size increased nearly 20-fold from 30.8 ± 2.8 to 592 ± 79 mm^3, an average of 2.12 ± 0.4-fold growth each 24-hr period. Changes in size of individual organs, however, were heterogeneous even to within subsets of the same tissue zones. The eye expanded exponentially at a constant rate, and grew an average of 2.24 times faster than the whole embryo over our interrogated range (Fig. 4E). Midbrain and forebrain growth were exponential but slower than that of the

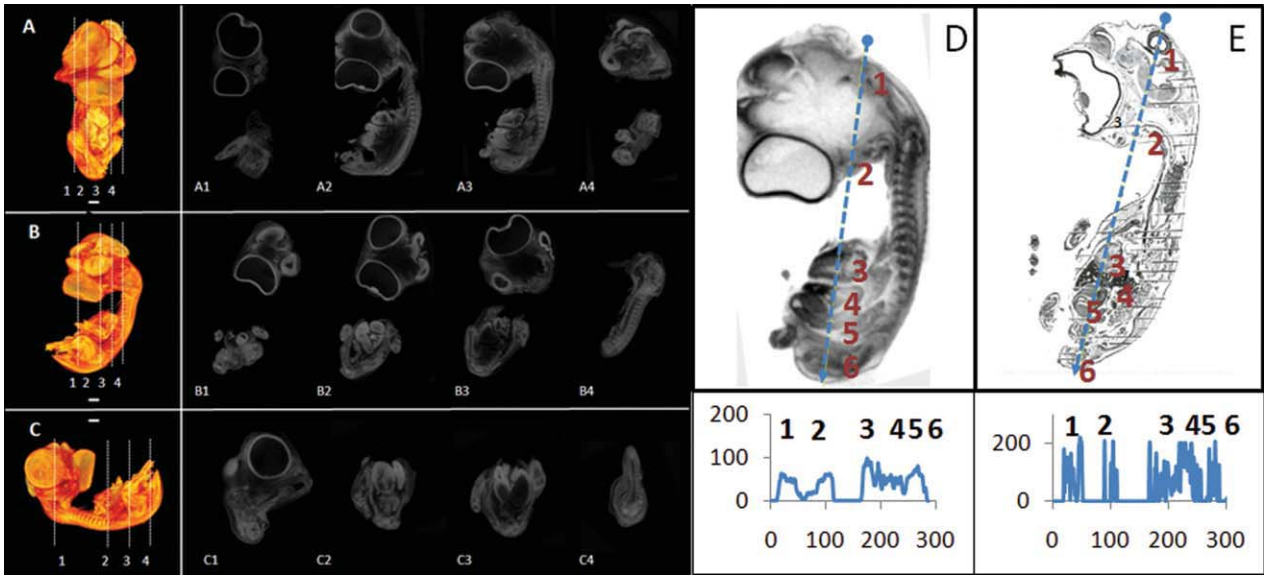

Fig. 3. 3D surface rendering and 2D digital sections of Day 10 chick embryos. Left panels are 3D isosurface renderings. Middle panels are 2D sections in (**A1**–**A4**) Sagittal, (**B1**–**B4**) coronal, and (**C1**–**C4**) axial planes. Right panels compare signal contrast of Micro-CT (**D**) with histology (**E**). Graphs below images contrast along lines in D and E, respectively. 1 = hindbrain, 2 = mandible, 3 = ventricle, 4 = liver, 5 = gizzard, 6 = tail. Scale bars (A, B, and C) = 1 mm.

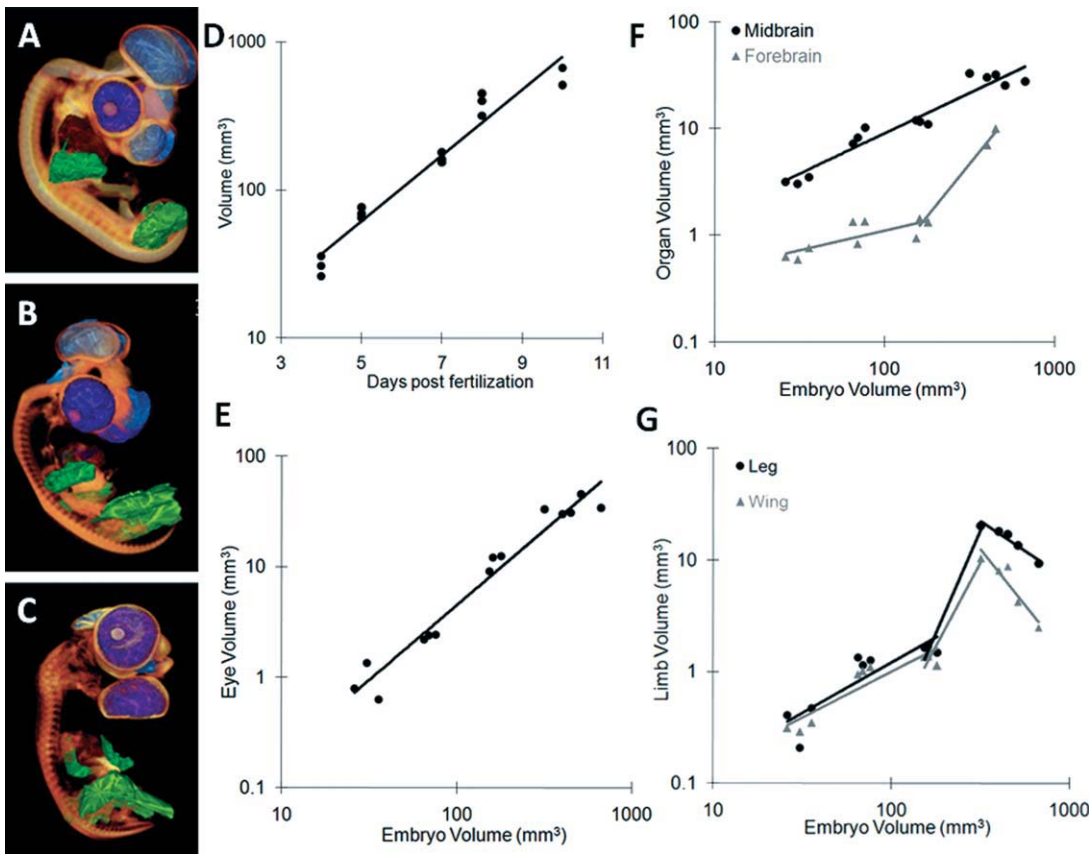

Fig. 4. Isosurface 3D renderings of Day 4 (**A**), Day 7 (**B**), and Day 10 (**C**) embryos. Colorized segmentations of cranial neural crest (light Blue), eyes (purple), limb (green), cardiac muscle (brown), and the conotruncal cavity (dark blue within the brown cardiac muscle) are highlighted. **D**: Volumetric embryonic growth versus embryonic stage. Quantification of eye (**E**), brain (**F**), and limb volume with respect to embryo volume. See Table 1 for regression parameters. Scale bars = 1 mm.

TABLE 1. Regression parameters for embryonic growth curves: $Y = mX^n$

Region	Range(s)	m	n	Fit (R^2)
Embryo	E4–E10	4.773	0.512	0.95
Midbrain	E4–E10	0.278	0.755	0.93
Forebrain	E4–E7	0.202	0.368	0.60
	E7–E10	6.00E–05	1.97	0.98
Eye	E4–E10	8.70E–03	1.36	0.96
Leg	E4–E7	1.88E–02	0.903	0.78
	E7–E8	1.00E–08	3.68	0.94
	E8–E10	1.04E + 04	−1.07	0.93
Wing	E4–E7	2.26E–02	0.822	0.84
	E7–E8	3.00E–07	2.99	0.93
	E8–E10	1.00E + 06	−2.01	0.87
Heart	E4–E10	2.65E–03	1.01	0.94
Left Atrium	E4–E7	8.50E–03	3.53	0.82
	E7–E10	1.58E–01	0.719	0.86
Right Atrium	E4–E7	9.00E–03	4.3	0.86
	E7–E10	3.14E–01	0.592	0.89
Left Ventricle	E4–E10	3.92E–01	1.07	0.98
Right Ventricle	E4–E10	4.89E–01	0.858	0.98
	E7–E10	6.00E–05	1.97	0.98

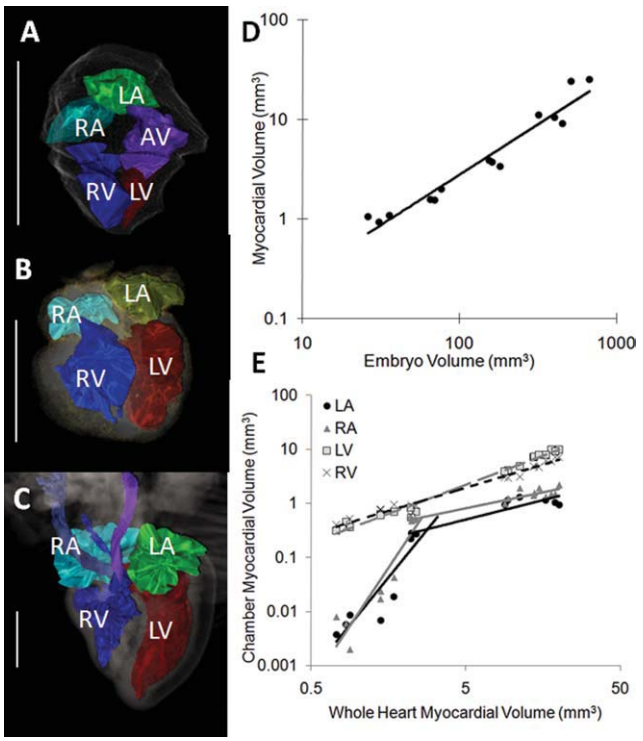

Fig. 5. 3D Segmentation and quantitative analysis of cardiac chambers at Day 4 (**A**), Day 7 (**B**), and Day 10 (**C**) acquired through Micro-CT. Scale bar = 1 mm. **D**: Quantification of whole heart myocardial growth between Day 4 and Day 12 relative to that of the whole embryo. **E**: Chamber specific myocardial growth curves relative to that of the whole heart.

whole embryo (Fig. 4F). Although the midbrain exponential growth rate was unchanged throughout the developmental window, forebrain growth accelerated relative to the embryo between Day 7 and Day 10. The forebrain increased from 0.6 ± 0.02 mm^3 at Days 4 to 1.975 ± 0.03 mm^3 at Day 10. Midbrain size remained at least 10 times larger than the forebrain size throughout the study period (26.37 ± 1.04 vs. 1.95 ± 0.02 mm^3 at Day 10). Although the midbrain was the largest region measured at Day 4 (3.23 ± 0.14 mm^3), the eye became the largest organ by Day 10 (39.7 mm^3), growing 10.1-fold in size between Day 4 and Day 7, and 3.7-fold from Day 7 to Day 10. We quantified three distinct phases for Leg and wing growth in the chick (Fig. 4G). The first phase, between Day 4 and Day 7, consisted of exponential growth that was slower relative to the whole embryo. A very rapid phase of growth transpired between Day 7 and Day 8, such that the wing grew nearly 7-fold and the leg grew over 11-fold. Although wing and leg buds were identical in size at Day 4 (0.3 ± 0.01 mm^3 vs. 0.31 ± 0.1 mm^3, respectively), leg size peaked at 18.5 ± 0.98 mm^3 by Day 8, twice the size of the wing on the same day (9.1 ± 0.7 mm^3). Leg volume then decreased 64% (wing) and 38% (leg) between Day 8 and Day 10. This period is commensurate with mesenchymal condensation and interdigitation through apoptosis.

We further analyzed the volumetric growth of the embryonic heart chambers and quantified changes in 3D myocardial tissue volume specific to each chamber between Day 4 and Day 12 (Fig. 5). Guided by anatomical landmarks within the lumen, we could clearly identify each cardiac segment as early as HH23 (Fig. 5A–C). Myocardial boundaries between chambers were established by extending the edge of the chamber-specific lumens (demarcated by the valves) perpendicularly through the walls. The atrial and ventricular septal walls were partitioned 50–50 between the left and right sides. Like the other organs, we here do not differentiate between cardiomyocyte and non-cardiomyocyte populations, or the amount and types of matrix, but labeled the entire tissue volumes as "myocardial." Our data shows myocardial growth was exponential, but at a constant rate approximately equivalent to that of the whole embryo. Heart myocardial size increased from 1.06 ± 0.05 mm^3 at Day 4 to 24.77 ± 0.41 mm^3 by Day 10 (Fig. 5D). Myocardial growth of individual cardiac chambers was heterogeneous relative to whole heart volume (Fig. 5E). Left and right atria myocardium grew in two phases: rapid growth between Day 4 and Day 7, followed by slower growth to Day 12. There was initially no difference between left and right atrial myocardial volume (0.006 ± 0.002 vs. 0.005 ± 0.003 mm^3, respectively). The right grew faster than the left until Day 7, and remained larger than the left by Day 12 (1.84 ± 0.49 vs. 0.98 ± 0.07 mm^3, respectively, $P < 0.05$). Ventricular growth rate was unchanged over the range assayed, and approximately equivalent to that of the whole heart. At Day 5, the right ventricular myocardium was significantly larger than the left (0.83 ± 0.10 vs. 0.65 ± 0.05 mm^3, $P < 0.05$), but Day 9 and onwards the left side has accumulated significantly more myocardium (9.6 ± 0.34 vs. 7.1 ± 0.03 mm^3 by Day 12, $P < 0.01$). These results paralleled our previously published results on cardiac chamber volume growth in the embryo, indicating that myocardial volume increases directly with lumen volume regardless of chamber (Butcher et al., 2007b). The relative deceleration of atrial myocardial accumulation compared to ventricular may be partially explained by the maturation of ventricular conduction patterns and increased proportion of diastolic inflow through ventricular suction.

TABLE 2. Comparison of quantitative imaging platforms for embryonic development

Platform	Resolution	Contrast agents?	Depth of field	Cost	Acquisition time	Live animals?
Micro-CT	<1–25 μm	Yes	<1–8 cm	$50–100/hr	0.05–5 hr	Yes
Ultrasound	30 μm	No	3–4 mm	$10–20/hr	n/a	Yes
Optical coherence tomography	1 μm	No	1–3 mm	n/a	12 hr	Yes
MR microscopy (μMRI)	25–100 μm	Yes	>10 cm	$400–600/hr	6–30 hr	Yes
Fluorescence microscopy	1 μm	Yes	0.05–0.1 mm	n/a	n/a	Yes
Laser microscopy	0.3 μm	Yes	0.2–1.0 mm	$10–20/hr	1–2 hr	Yes
Optical projection tomography	0.3 μm	Yes	>10 mm	$10–20/hr	1–2 hr	No
Serial section histology	<1 μm (in plane)	Yes	n/a	n/a	3–4 hr	No

DISCUSSION

Embryonic morphogenesis is a rapid and complex process occurring on multiple length scales. Genetic and experimental perturbation of development in small animal models has provided the majority of our understanding morphological events and their underlying biological mechanisms. The majority of these prior experiments have created and studied early embryonic non-survivable defects that have limited relevance to clinical cases. Many clinically significant malformations may have subtle presentations during embryonic development that are challenging to discover. Instead of the absence of a tissue, its growth or positioning may be altered. Identifying these details requires quantitative phenotype screening technologies. The traditional and still most common imaging approach is microtome section histology. Quantification and interpretation of morphologic features with this method, however, is highly sensitive to fixation and processing methods, as well as small deviations in sectioning plane. Digitally reconstructing serial sections into three-dimensional volumes has improved this approach, but is heavily time consuming and ineffective for screening. Furthermore, complex and tortuous geometries are often under-resolved because of the unrecorded out-of-plane information. Small animal volumetric imaging technologies such as ultrasound biomicroscopy, micro-MRI, and micro-CT have been employed to quantify adult and embryonic anatomy, with varying degrees of effectiveness (Table 2).

We and others have used pre-clinical ultrasound to visualize cardiac dynamics in developing chick and mouse embryos (Broekhuizen et al., 1999; Phoon, 2001; Butcher et al., 2007a). Ultrasound has the advantage of high ungated temporal resolution (over 250 frames/sec), but can also be gated for better resolution. For small animals, information gained is almost exclusively 2D with spatial resolution ~30–50 μ. Contrast for ultrasound is challenging in embryos, as microbubble size is not negligible in relation to vessel diameter and are challenging to inject (Alter et al., 2009). 3D micro-MRI manipulates intrinsic magnetic properties of tissues to generate contrast and can achieve spatial resolutions less than 20 μ for fixed tissues. In addition, manipulation of electron spins with magnetic stimulation can help improve tissue contrast locally without the need of exogenous dyes. Isotropic voxel size, however, is inversely proportional to the size of the volume interrogated, which limits the ability to image larger samples with high 3D detail without long scan times (Li et al., 2007).

Microcomputed Tomography (Micro-CT) generates images by resolving X-ray attenuation through a specimen similar to clinical X-rays. Both X-ray source and imaging camera are rotated around the specimen. Micro-CT is attractive because (A) there are no registration artifacts, (B) spatial resolutions approach 1 μm voxel resolution, and (C) the size of the object to be imaged is limited only by the bore of the machine. With scan times as low as a few minutes (for 25 μ resolution) and the ability to image multiple embryos simultaneously, MicroCT is a versatile imaging platform well suited for small animal imaging. We previously established its utility for quantifying avian cardiovascular development, showing comparable resolution with scanning electron microscopy and better rendering of tortuous geometry like outflow tract and myocardial trabeculation (Butcher et al., 2007b). Higher resolution scans of as low as 1 μm voxel size are possible, which could help resolve finer anatomical details, but at a cost of field of view and the inability to image live specimens.

A persistent challenge, however, was the limited ability to visualize and quantify soft tissues using Micro-CT. We and others have overcome this limitation with the optimization of osmium tetroxide (OT) as a CT dense contrast agent, showing dramatic visualization capability in mouse embryos without altering specimen geometry (Johnson et al., 2006; Metscher, 2009; Degenhardt et al., 2010). This study complements these by quantitatively analyzing embryonic chick morphogenesis. We developed a simple two-phased approach for OT contrast enhancement. Our preliminary experiments found that the time required for complete penetration varied between stages. This is potentially because OT preferentially binds fatty acids, which may impede further diffusion. We found that prolonged incubation of a sample in OT maintained contrast with only a slight increase in risk of brittle fracture, earliest stages being most susceptible. We also found that perfusing through a vessel at Day 8 and later significantly reduced the time required for complete penetration, potentially because endothelial permeability is greater than epithelial at these stages and/or larger surface area for diffusion via internal vessels. The two-stage approach (straight diffusion or with perfusion) presented here was the shortest protocol that achieved optimal contrast at all stages and organs analyzed. Other heavy metal agents like uranylacetate that selectively bind proteins may also return good contrast, but have not been tried in this study. Micro-CT generated virtual 2D "sections" were quantitatively similar in tissue boundary delineations and qualitatively similar in intra-tissue contrast as histological sections, agreeing

with recent observations in mouse and quail embryos. Histological sections were more accurate than Micro-CT for resolving small (<25 μm) features because resolution is limited only by the quality of the optics. Micro-CT however can instantly render any sectioning plane from the same embryo, which is advantageous when screening for morphological variations as not all anatomical features are clearly visualized in one plane. This is of increasing importance as more subtle congenital phenotypes are being identified studied for long term consequences.

The results presented in this study establish baseline volumetric growth information for embryonic chick from which effects of experimental treatments be compared. Most previous 3D imaging studies focus on optimizing tissue contrast levels, but less attention has been paid to quantifying morphology, likely due to the onerous task of acquiring, tracing, and converting 2D section images into 3D volumes. Among the more rigorous detailed embryonic growth information is a series of papers by Goedbloed (Goedbloed, 1972, 1980). He quantified growth of many organs in embryonic mouse and rat, including brain, heart, and eye as in our study. He found that rodent embryonic growth decelerated with time, which contrasts our chick data that supports constant growth rates. As in our study, he found that eye and heart growth was exponential and proportional with whole embryo growth. Exponential growth in the murine telencephalon slowed at E13, which was the equivalent time that we found a change in growth in chick (Day 7) except that we record acceleration afterwards. The precise meaning is unclear, as our forebrain measurements included the diencephalon while the Goedbloed study did not. Also, our data suggests chick forebrain growth is slower than the mouse prior to Day 7. Heart growth was exponential in both the chick and rodent studies, and paralleled embryonic growth to the same degree. This growth pattern may therefore be a conserved requirement for normal developmental progression. Our previous data quantifying cardiac lumen volumes with Micro-CT also showed exponential growth between Day 4 and Day 10 (Butcher et al., 2007b). Goedbloed reported slower exponential growth of the rodent eye in comparison to our chick data, which is expected since the rodent eye is proportionally smaller in the rodent than chick during this developmental window. Goodall and colleagues reported linear volumetric growth in the eye between Day 4 and Day 10 using MRI, with final eye volumes three times what we report (Goodall et al., 2009). They injected liquid contrast directly into the eye, which may have increased their volumes, and it is unclear whether more than one sample was used per stage. As an additional comparison we measured the volume of chick eyes at Day 10 from histological sections, and found volumes nearly identical to our Micro-CT imaging (45 mm^3). Li et al. imaged chick and quail limb development using 3D μMRI, but no quantitative analyses were performed (Li et al., 2007). Our study was also able to document volume reduction during growth, particularly in the limb during digit formation as suggested by others (Hurle and Ganan, 1987; Wagner, 2005). Finally, we identified chamber specific myocardial growth curves for embryonic chick heart, and found novel trends between atrial and ventricular chambers and between left and right sided chambers. It is well known that hemodynamics is an important regulator of cardiac growth and remodeling (Reckova et al., 2003), and that hemodynamic forces are continually changing during cardiogenesis (Hu and Clark, 1989; Phoon, 2001; Butcher et al., 2007a). Our data shows that right ventricular myocardium volume is larger at Day 4, but the left side dominates by Day 10. Our previous ventricular lumen data showed that the left side was consistently larger than the right throughout development. Ventricular myocardial volumes were initially only 60% of lumen volumes, but increased such that by Day 10 were equal to or larger. Ventricular myocardium/lumen ratio was not significantly different between sides at any stage of development. Although the meaning of this finding is not yet known, it suggests that this proportionality may be important for efficient hemodynamic function. The growth changes make sense however because previous studies demonstrate a significant amount of tissue volume is being added via proepicardial (both ventricles), neural crest (right ventricle, outflow tracts), and the secondary heart field during this time (Mjaatvedt et al., 2001; Yelbuz et al., 2003; Wessels and Perez-Pomares, 2004). Atrial lumen volumes, in contrast, grew much larger than their respective myocardium. Our data suggests that the right atrial myocardium thins while the left thickens, which makes sense since it will eventually pump greater hemodynamic loads (Butcher et al., 2007b). It is important to note that growth occurs via cell proliferation, hypertrophy, and matrix synthesis and remodeling. Although Micro-CT can account for the presence of tissue and voids, it cannot establish causes.

Collectively, our results demonstrate that fine morphological details as well as quantitative volumetric information can be obtained with Micro-CT imaging. The intrinsically digital information gained through Micro-CT can be readily applied for additional quantitative understanding of embryonic development. For instance, high detail finite element models can be created from these images to quantify mechanical and fluid dynamic aspects of embryonic development beyond what has been done recently in the embryonic heart lumen (Wang et al., 2009). An important but still challenging extension of these results is quantitative imaging of living embryos. Davis et al. developed a spectral domain optical coherence tomography system for *in vivo* volumetric imaging for the chicken embryo heart in order to further analyze congenital heart disease (Davis et al., 2008). Holmes et al. used Micro-MRI to serially image embryonic chick growth and cardiac function in ovo (Holmes et al., 2009). Badea et al. reported micro CT based cardiac morphological and functional imaging in mice and rats using both prospective and retrospective gating approaches using injectable iodinylated contrast agents (Badea et al., 2008). Rabin et al. developed a heavy metal based nanoparticle contrast agent for *in vivo* imaging (Rabin et al., 2006). Applying contrast agents like these can further extend Micro-CT imaging of embryonic development to 4D (3D in space at short time scales like cardiac cycle) and 5D (3D in space with cardiac beating and longitudinal growth). It will be critical to establish benchmarks for how much X-ray dose live embryos can tolerate, which will likely be developmental stage dependent. In this study, we applied X-Ray energies and acquisition parameters that based on prior studies in mouse could maintain viability, but an

analysis in chick so far has not been done. Retrospective gating techniques for organisms that do not present a tractable ECG signal have been developed (Liebling et al., 2005), but their adaptability to commercial Micro-CT acquisition protocols is uncertain.

ACKNOWLEDGMENTS

The authors thank Del and Craig Shelley (GE Healthcare) and Drew Noden (Cornell University) for their technical expertise. They also thank Charles Keller and Suresh Prajapati (UTHSCSA) for their expert comments.

LITERATURE CITED

Alter J, Sennoga CA, Lopes DM, Eckersley RJ, Wells DJ. 2009. Microbubble stability is a major determinant of the efficiency of ultrasound and microbubble mediated in vivo gene transfer. Ultrasound Med Biol 35:976–984.

Badea CT, Drangova M, Holdsworth DW, Johnson GA. 2008. In vivo small-animal imaging using micro-CT and digital subtraction angiography. Phys Med Biol 53:R319–R350.

Bain MM, Fagan AJ, Mullin JM, McNaught I, McLean J, Condon B. 2007. Noninvasive monitoring of chick development in ovo using a 7T MRI system from day 12 of incubation through to hatching. J Magn Reson Imaging 26:198–201.

Bellairs R, Osmond M. 2005. The atlas of chick development. 2nd ed. New York, USA: Academic Press.

Borue X, Noden DM. 2004. Normal and aberrant craniofacial myogenesis by grafted trunk somitic and segmental plate mesoderm. Development 131:3967–3980.

Broekhuizen ML, Hogers B, DeRuiter MC, Poelmann RE, Gittenberger-de Groot AC, Wladimiroff JW. 1999. Altered hemodynamics in chick embryos after extraembryonic venous obstruction. Ultrasound Obstet Gynecol 13:437–445.

Butcher JT, McQuinn TC, Sedmera D, Turner D, Markwald RR. 2007a. Transitions in early embryonic atrioventricular valvular function correspond with changes in cushion biomechanics that are predictable by tissue composition. Circ Res 100:1503–1511.

Butcher JT, Sedmera D, Guldberg RE, Markwald RR. 2007b. Quantitative volumetric analysis of cardiac morphogenesis assessed through micro-computed tomography. Dev Dyn 236:802–809.

Camenisch TD, Schroeder JA, Bradley J, Klewer SE, McDonald JA. 2002. Heart-valve mesenchyme formation is dependent on hyaluronan-augmented activation of ErbB2–ErbB3 receptors. Nat Med 8:850–855.

Carney EW, Tornesi B, Keller C, Findlay HA, Nowland WS, Marshall VA, Ozolins TR. 2007. Refinement of a morphological scoring system for postimplantation rabbit conceptuses. Birth Defects Res B Dev Reprod Toxicol 80:213–222.

Clark KL, Yutzey KE, Benson DW. 2006. Transcription factors and congenital heart defects. Annu Rev Physiol 68:97–121.

Davis AM, Rothenberg FG, Shepherd N, Izatt JA. 2008. In vivo spectral domain optical coherence tomography volumetric imaging and spectral Doppler velocimetry of early stage embryonic chicken heart development. J Opt Soc Am A Opt Image Sci Vis 25:3134–3143.

Degenhardt K, Wright AC, Horng D, Padmanabhan A, Epstein JA. 2010. Rapid 3D phenotyping of cardiovascular development in mouse embryos by micro-CT with iodine staining. Circ Cardiovasc Imaging 3:314–322.

Dhenain M, Ruffins SW, Jacobs RE. 2001. Three-dimensional digital mouse atlas using high-resolution MRI. Dev Biol 232:458–470.

Goedbloed JF. 1972. The embryonic and postnatal growth of rat and mouse. I. The embryonic and early postnatal growth of the whole embryo. A model with exponential growth and sudden changes in growth rate. Acta Anat (Basel) 82:305–306.

Goedbloed JF. 1980. Embryonic and postnatal growth of the rat and mouse. VI. Prenatal growth of organs and tissues: individual organs; final remarks on parts I-VI, phase transitions. Acta Anat (Basel) 106:108–128.

Goodall N, Kisiswa L, Prashar A, Faulkner S, Tokarczuk P, Singh K, Erichsen JT, Guggenheim J, Halfter W, Wride MA. 2009. 3-Dimensional modelling of chick embryo eye development and growth using high resolution magnetic resonance imaging. Exp Eye Res 89:511–521.

Hogers B, DeRuiter MC, Gittenberger-de Groot AC, Poelmann RE. 1999. Extraembryonic venous obstructions lead to cardiovascular malformations and can be embryolethal. Cardiovasc Res 41:87–99.

Hogers B, van der Weerd L, Olofsen H, van der Graaf LM, DeRuiter MC, Gittenberger-de Groot AC, Poelmann RE. 2009. Non-invasive tracking of avian development in vivo by MRI. NMR Biomed 22:365–373.

Holmes WM, McCabe C, Mullin JM, Condon B, Bain MM. 2009. In ovo non-invasive quantification of the myocardial function and mass of chick embryos using magnetic resonance imaging. NMR Biomed 22:745–752.

Hu N, Christensen DA, Agrawal AK, Beaumont C, Clark EB, Hawkins JA. 2009. Dependence of aortic arch morphogenesis on intracardiac blood flow in the left atrial ligated chick embryo. Anat Rec (Hoboken) 292:652–660.

Hu N, Clark EB. 1989. Hemodynamics of the stage 12 to stage 29 chick embryo. Circ Res 65:1665–1670.

Hurle JM, Ganan Y. 1987. Formation of extra-digits induced by surgical removal of the apical ectodermal ridge of the chick embryo leg bud in the stages previous to the onset of interdigital cell death. Anat Embryol (Berl) 176:393–399.

Johnson JT, Hansen MS, Wu I, Healy LJ, Johnson CR, Jones GM, Capecchi MR, Keller C. 2006. Virtual histology of transgenic mouse embryos for high-throughput phenotyping. PLoS Genet 2:e61.

Li X, Liu J, Davey M, Duce S, Jaberi N, Liu G, Davidson G, Tenent S, Mahood R, Brown P, Cunningham C, Bain A, Beattie K, McDonald L, Schmidt K, Towers M, Tickle C, Chudek S. 2007. Micro-magnetic resonance imaging of avian embryos. J Anat 211:798–809.

Liebling M, Forouhar AS, Gharib M, Fraser SE, Dickinson ME. 2005. Four-dimensional cardiac imaging in living embryos via postacquisition synchronization of nongated slice sequences. J Biomed Opt 10:054001.

Maciaczyk J, Singec I, Maciaczyk D, Klein A, Nikkhah G. 2009. Restricted spontaneous in vitro differentiation and region-specific migration of long-term expanded fetal human neural precursor cells after transplantation into the adult rat brain. Stem Cells Dev 18:1043–1058.

Martinez HG, Prajapati SI, Estrada CA, Jimenez F, Quinones MP, Wu I, Bahadur A, Sanderson A, Johnson CR, Shim M, Keller C, Ahuja SS. 2009. Images in cardiovascular medicine: microscopic computed tomography-based virtual histology for visualization and morphometry of atherosclerosis in diabetic apolipoprotein e mutant mice. Circulation 120:821–822.

McBride KL, Pignatelli R, Lewin M, Ho T, Fernbach S, Menesses A, Lam W, Leal SM, Kaplan N, Schliekelman P, Towbin JA, Belmont JW. 2005. Inheritance analysis of congenital left ventricular outflow tract obstruction malformations: segregation, multiplex relative risk, and heritability. Am J Med Genet A 134:180–186.

Metscher BD. 2009. MicroCT for comparative morphology: simple staining methods allow high-contrast 3D imaging of diverse non-mineralized animal tissues. BMC Physiol 9:11.

Mjaatvedt CH, Nakaoka T, Moreno-Rodriguez R, Norris RA, Kern MJ, Eisenberg CA, Turner D, Markwald RR. 2001. The outflow tract of the heart is recruited from a novel heart-forming field. Dev Biol 238:97–109.

Munoz-Sanjuan I, Simandl BK, Fallon JF, Nathans J. 1999. Expression of chicken fibroblast growth factor homologous factor (FHF)-1 and of differentially spliced isoforms of FHF-2 during development and involvement of FHF-2 in chicken limb development. Development 126:409–421.

Niswander L. 2002. Interplay between the molecular signals that control vertebrate limb development. Int J Dev Biol 46:877–881.

Olson EN. 2004. A decade of discoveries in cardiac biology. Nat Med 10:467–474.

Phoon CK. 2001. Circulatory physiology in the developing embryo. Curr Opin Pediatr 13:456–464.

Rabin O, Manuel Perez J, Grimm J, Wojtkiewicz G, Weissleder R. 2006. An X-ray computed tomography imaging agent based on long-circulating bismuth sulphide nanoparticles. Nat Mater 5:118–122.

Ruffins SW, Martin M, Keough L, Truong S, Fraser SE, Jacobs RE, Lansford R. 2007. Digital three-dimensional atlas of quail development using high-resolution MRI. Sci World J 7:592–604.

Smith BR, Linney E, Huff DS, Johnson GA. 1996. Magnetic resonance microscopy of embryos. Comput Med Imaging Graph 20: 483–490.

Snider P, Hinton RB, Moreno-Rodriguez RA, Wang J, Rogers R, Lindsley A, Li F, Ingram DA, Menick D, Field L, Firulli AB, Molkentin JD, Markwald R, Conway SJ. 2008. Periostin is required for maturation and extracellular matrix stabilization of noncardiomyocyte lineages of the heart. Circ Res 102:752–760.

Wagner GP. 2005. The developmental evolution of avian digit homology: an update. Theor Biosci 124:165–183.

Wang Y, Dur O, Patrick MJ, Tinney JP, Tobita K, Keller BB, Pekkan K. 2009. Aortic arch morphogenesis and flow modeling in the chick embryo. Ann Biomed Eng 37:1069–1081.

Wenink AC. 1992. Quantitative morphology of the embryonic heart: an approach to development of the atrioventricular valves. Anat Rec 234:129–135.

Wessels A, Perez-Pomares JM. 2004. The epicardium and epicardially derived cells (EPDCs) as cardiac stem cells. Anat Rec A Discov Mol Cell Evol Biol 276:43–57.

Williams BS, Doyle MD. 1996. An Internet atlas of mouse development. Comput Med Imaging Graph 20:433–447.

Yelbuz TM, Waldo KL, Zhang X, Zdanowicz M, Parker J, Creazzo TL, Johnson GA, Kirby ML. 2003. Myocardial volume and organization are changed by failure of addition of secondary heart field myocardium to the cardiac outflow tract. Dev Dyn 228:152–160.

Zhang X, Yelbuz TM, Cofer GP, Choma MA, Kirby ML, Johnson GA. 2003. Improved preparation of chick embryonic samples for magnetic resonance microscopy. Magn Reson Med 49:1192–1195.